Received: 14 October 2017 | Revised: 25 November 2017 | Accepted: 18 December 2017

DOI: 10.1002/jrs.5333

SPECIAL ISSUE - RESEARCH ARTICLE

WILEY Journal of RAMAN SPECTROSCOPY

Surface-enhanced micro-CARS mapping of a nanostructured cerium dioxide/aluminum film surface with gold nanoparticle-bound organic molecules

Viktor I. Fabelinsky[1] | Dimitrii N. Kozlov[1] | Sergey N. Orlov[1] | Yury N. Polivanov[1] | Ivan A. Shcherbakov[1] | Valery V. Smirnov[1] | Konstantin A. Vereschagin[1] | Grigory M. Arzumanyan[2] | Kahramon Z. Mamatkulov[2] | Konstantin N. Afanasiev[3] | Andrey N. Lagarkov[3] | Ilya A. Ryzhikov[3] | Andrey K. Sarychev[3] | Igor A. Budashov[4] | Natalia L. Nechaeva[4] | Ilya N. Kurochkin[5]

[1] A.M. Prokhorov General Physics Institute, Russian Academy of Sciences, Vavilov str. 38, 119991 Moscow, Russia

[2] Joint Institute for Nuclear Research, Joliot-Curie str. 6, 141980 Dubna, Moscow Region, Russia

[3] Institute for Theoretical and Applied Electromagnetics, Russian Academy of Sciences, Izhorskaya str. 13, 125412 Moscow, Russia

[4] Chemistry Department, M.V. Lomonosov Moscow State University, Leninskiye Gory 1-3, 119991 Moscow, Russia

[5] N.M. Emanuel Institute of Biochemical Physics, Russian Academy of Sciences, Kosygin str. 4, 119334 Moscow, Russia

Correspondence
Dimitrii N. Kozlov, A.M. Prokhorov General Physics Institute, Russian Academy of Sciences, Vavilov str. 38, 119991 Moscow, Russia.
Email: dnk@kapella.gpi.ru

Funding information
The Presidium of Russian Academy of Sciences, Grant/Award Number: Basic Research Program № I.16; Joint Institute for Nuclear Research, Grant/Award Number: Thematic Project "Multimodal optical platform"; Russian Academy of Sciences

Abstract

Highly contrast epi-surface-enhanced coherent anti-Stokes Raman scattering (SECARS) microimages of Au-nanoparticle-bound organic reporter molecule distributions at a surface of novel surface-enhanced Raman scattering (SERS)-active metamaterial junctions, based on nanoparticles spread over a nanostructured CeO_2 faceted dielectric film, deposited on an Al sublayer, were recorded at two-color picosecond excitation of the surface in the near-infrared spectral range. For this, a scanning confocal laser-based micro-CARS spectrometer was employed. The investigations showed that at Raman resonant laser excitation of the molecules/Au-NP conjugates immobilized on the surface strong SECARS signals can be generated with laser powers not deteriorating the conjugates. Coupling CARS with the plasmonic metamaterial structures under investigation provided excellent chemical imaging contrast (up to 400) for biochemically relevant 5-thio(2-nitrobenzoic acid) and 4-mercaptophenylboronic acid reporter molecules. Taking into account easy handling and utmost long-term stability of the investigated metamaterial junction at ambient conditions, it might be considered as a promising perspective for a single-molecule-sensitivity surface-enhanced Raman scattering or SECARS biosensor.

KEYWORDS

SECARS, metamaterial, Au-nanoparticles, CeO_2, biosensor

1 | INTRODUCTION

A new surface-enhanced Raman scattering (SERS)-active metamaterial junction based on gold nanoparticles (NPs) spread over the surface of a nanostructured cerium dioxide (CeO_2) faceted dielectric film, deposited on a thin aluminum sublayer, has been recently proposed and investigated.[1,2] Based on the results of confocal micro-

Raman spectroscopy mapping of the CeO_2 surface structure at the 456 cm^{-1} CeO_2 characteristic Raman line by using a 1-μm diameter spot of 532-nm continuous-wave (cw) laser radiation, it has been reported that the nanostructured CeO_2 films provide inhomogeneous distribution of an electromagnetic field intensity in the transmitted and reflected light. Theoretical considerations allowed to conclude that in this case, the film should enable additional amplification of the intensity of spontaneous Raman scattering by molecules localized at the metamaterial surface. The investigated Au-NPs/CeO_2/Al structures were reported to show surface enhancement of spontaneous Raman scattering of 785-nm cw laser radiation by 5-thio(2-nitrobenzoic acid) (TNB), molecules bound to Au-NPs. The TNB molecule was taken as a model for a reporter molecule being of interest for biochemical and immunological analysis. The enhancement factor was found to depend on the CeO_2 film thickness. It should be noted that one of the attractive features of the proposed novel structure is the reported outstanding stability—for months—of its Raman-enhancing properties, even if stored in room air at ambient conditions.

The Au-NPs/CeO_2/Al structures can be assumed to enhance local laser fields involved into the four-wave mixing process of coherent anti-Stokes Raman scattering (CARS) by the reporter molecules. Hence, they can be expected to demonstrate surface-enhanced CARS (SECARS) activity. After the first experimental observations[3–5] and theoretical description,[6] SECARS-spectroscopy in recent times generates more and more research activities that are shortly summarized in the review papers.[7–9] These activities, among others, are devoted to studying of peculiarities of SECARS itself,[10–13] to biomedical applications,[14–17] to finding the ways to reach a single-molecule sensitivity,[15,18,19] which with SECARS may be achievable for a much broader variety of substances than with classical SERS, due to potentially higher field enhancing factors,[9,11] and even to investigations of arising possibility to engineer SERS-active structures delivering the highest gain in the SECARS configuration.[20–22] But the field of the most interesting SECARS applications opens when the capability of the technique to be employed in femto- and picosecond time-resolved experiments is realized. This already led to an impressive direct observation of vibrations of a single molecule[19] and of other exciting features of ultrafast SECARS.[23]

But as it has been figured out by Crampton et al.,[23] the dynamic range of laser power between detection and destruction of a metal particle/reporter molecule complex in case of transient (femto- or picosecond) SECARS study is rather small. Hence, searching of new optical field enhancing structures, which demonstrate stable and reproducible single-molecule SECARS sensitivity, is an actual and challenging task.

The present work is the first experimental study of feasibilities and limitations to detect SECARS signals from biochemically relevant TNB and 4-mercaptophenylboronic acid (MPBA) reporter molecules bound to Au-NPs, which are immobilized on the surface of the CeO_2 faceted dielectric film deposited on a thin Al layer, by employing a novel scanning confocal picosecond laser-based micro-CARS spectrometer. For this, we aimed to perform the mapping of the SECARS intensity at the characteristic Raman shifts of TNB (1,338 cm^{-1}) and MPBA (1,571 cm^{-1}) molecules, that is, recording microimages of the film surface at the corresponding anti-Stokes wavelengths, using the excitation of the surface in the near-infrared spectral range within a 1-μm diameter spot. Furthermore, we intended to evaluate the nondestructive sample surface excitation level, to compare the Raman resonant and nonresonant (background) SECARS signal intensities and to estimate the imaging contrast, to record SERS microimages of the metamaterial sample areas and compare them with those recorded using SECARS.

2 | EXPERIMENTAL

2.1 | Micro-CARS spectrometer

SECARS signals and microimages were recorded using a scanning confocal laser micro-CARS spectrometer "Confotec CARS" (see the schematic in Figure 1) with high spatial resolution and high laser spot scanning rate.

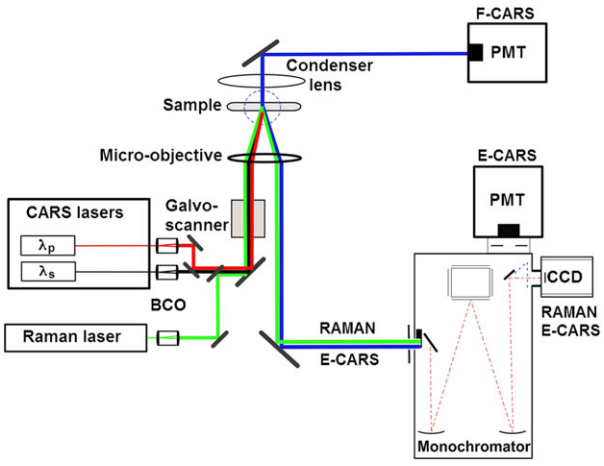

FIGURE 1 Schematic of the scanning confocal laser micro-CARS spectrometer "Confotec CARS". Going along the optical axis and overlapping pump, Stokes and epi-CARS beams are shown off-axis for visibility. The micro-objective designated on the picture is in fact the part of the Nikon TE2000S inverted microscope.
CARS = coherent anti-Stokes Raman scattering;
PMT = photomultiplier tube; BCO = beam collimating optics
[Colour figure can be viewed at wileyonlinelibrary.com]

The system, developed, designed, and manufactured by SOL Instruments Ltd. (Belarus), is based on a Nd^{3+}:YVO_4 diode-pumped picosecond passively mode-locked laser (1,064 nm, 7 ps, 85 MHz, 5 W) and an optical parametric oscillator (OPO) (PT257-SOPO, EKSPLA, Lithuania), synchronously pumped by the frequency-doubled radiation of this laser (2 W at 532 nm). The signal wave of the OPO (690–990 nm, 6 ps, 150–350 mW) was used as pump, whereas a part of a 1,064-nm beam—as Stokes radiation in the CARS process. A temperature-controlled lithium triborate (LBO) crystal and a Lyot filter are employed in the parametric oscillator for tuning the pump wavelength. The linewidth of the pump radiation is ~5–7 cm^{-1}, whereas the OPO tuning range allows the Raman shifts, potentially achievable in CARS experiments, to be 700–5,000 cm^{-1}. The OPO wavelength is determined by the readings of the precalibrated OPO control unit.

Pump and Stokes beams of parallel polarizations are collinearly overlapped using folding mirrors and diaphragms. The beams are focused on the sample using a NIKON TE2000S inverted microscope with (among others) an Olympus 40× 0.6 NA objective to a ~1-μm diameter spot with the depth of field ~1.6 μm. The focal spots are equalized in diameters by means of beam collimating optics installed into the beams. At epi-detection, as in our experiments, CARS radiation, at the anti-Stokes wavelength $\lambda_{aS} = \frac{\lambda_p}{(2-\lambda_p/\lambda_S)}$, where λ_p and λ_S are, respectively, the pump and Stokes radiation wavelengths, goes in the backward direction and is collected by the same objective. Propagating along the axis of the pump beams, the radiation is reflected by a dichroic mirror, transparent for the pump beams. Further on, the anti-Stokes light is spectrally separated from the pump radiation using two multilayer dielectric bandpass filters (FF01-794/160-25, Semrock) with the coefficients of suppression of $>10^6$ each and is directed to the entrance slit of a grating monochromator/spectrograph (MS 5004i, Solar TII, Belarus) with interchangeable gratings. As the slit, an iris diaphragm with a computer-driven opening (0.05–2 mm) is employed. A 150 grooves/mm or a 600 grooves/mm grating in the first order is used in the 520 mm focal length monochromator that provides the dispersion 12.6 and 3.17 nm/mm, respectively. The spectral characteristics of the anti-Stokes radiation transmitting optics ensure its detection within the Raman shift range of 990–3580 cm^{-1}. The monochromator has two output ports. Switching of the anti-Stokes signal beam between the ports is performed by a computer-driven folding mirror. In one of the ports, a multialcali-photocathode cooled photomultiplier tube (PMT) module (180–900 nm, H7844, Hamamatsu) is installed. An iris diaphragm with a computer-driven opening is mounted in front of the PMT window. The 16-bit analog-to-digital converter (ADC)-digitized PMT module signal is supplied to the computer.

A cooled Si 24.6 × 1.46 mm charge-coupled device (CCD)-matrix photodetector (HS 101H, PROSCAN, Belarus), with 2,048 × 122 elements, 12 μm × 12 μm each, and a 16-bit ADC, is installed in another port. The "full binning" mode of the detector is used, that is, the charge in each of the columns is accumulated, so that the detector is operating as a linear array. It has been experimentally established that around 830–850 nm the overall sensitivity of the detection system with the CCD detector is about 10^2 times higher than that with the PMT.

Scanning of the laser spot across the surface areas of maximum up to 330 μm × 330 μm with a spatial resolution up to 1,000 × 1,000 pixels, while detecting the CARS signal from the surface at a given Raman shift (signal mapping), is performed using galvo-driven mirrors that deflect the beams in front of the objective. Two mapping modes can be realized.

1. In the "fast-mapping" mode, the galvo-scanner continuously moves the laser beams across the selected surface area (typically, 24 μm × 24 μm in our case) during ~600 ms. As a result, a signal matrix (frame) of 251 × 251 pixels (~0.1 μm/pixel), totally 63,000 pixels, is generated with the exposure time of 10 μs/pixel. Within this time interval, the signal is detected by the PMT and digitized. Further on, a definite number of sequentially detected frames (30 in our case) are accumulated pixel by pixel. This image detection mode is preferable when the signal level is high enough, since it, first, allows the highest spatial resolution to be realized and, second, ensures significantly lower radiation and, especially, thermal load on the sample surface.
2. In the "slow-mapping" mode, the galvo-scanner moves the focal spot of the laser beams across the selected surface area by steps of about 0.5 or 1 μm. In this mode, in each position, the signal is accumulated, during the preset exposure time (typically, 0.5–1 s in our case), by the CCD-array, because the PMT signal accumulation during ~1 s is not provided by the electronics. Then, the focal spot is shifted to the next position. At the step of 0.5 μm, exposure of 1 s, and the mapping area dimensions of 24 μm × 24 μm, the mapping time amounts 40 min.

It should be noted that being equipped with two additional lasers—a 22 mW single-frequency 532 nm cw DPSS laser (SLM-417, Laser-Compact, Russia) and a 10 mW 633 nm He-Ne laser (05-LHP-991, Melles-Griot)—the presented spectrometer configuration provides also the

possibility to record Raman and SERS spectra. The additional laser beams are collinearly overlapped with the pump and Stokes beams and are adjusted to have the same focal spot diameters. Thus, all the signals are obtained from the same point of the sample surface with an accuracy of ~0.1–0.2 μm. It should be noted that the OPO output at 785 nm wavelength can also be used as a Raman and SERS pump source. In addition, the configuration allows forward-CARS mapping to be performed as well (see Figure 1), but this option was not employed in our experiments.

The micro-CARS spectrometer is manufactured in a way that switching between epi-CARS and Raman modes of operation, and between three Raman excitation wavelengths is provided by the computer that automatically changes the necessary mirror set after pushing a single button. Also important is that the geometrical beam paths for the detected anti-Stokes CARS and Stokes Raman radiation are exactly the same. This facilitates the direct comparison between CARS and Raman signal intensities, if necessary.

2.2 | SERS-active Au-NPs/CeO_2/Al metamaterial junctions

The procedures of the faceted CeO_2 films of Au-NPs and of Au-NP/reporter-molecule conjugates manufacturing, as well as of the conjugates immobilization on the film surface, are descried in details in previous papers.[1,2] Briefly, the investigated metamaterial structures are prepared on a 0.5 mm-thick ceramic alumina (Al_2O_3) substrate by deposition of an Al sublayer, with a thickness of 100–150 nm, and then of a CeO_2 film of a controllable thickness (in our case, 1,900 and 2,400 nm) by electron-beam evaporation. Nanoscale crystallites of CeO_2 form larger agglomerates that define a faceted structure of the CeO_2 film. Characteristic facet transversal dimensions are ~1.0–2.5 μm in dependence of a CeO_2 film thickness. Facets are surrounded by a kind of a ~100-nm high curb along their perimeter and are separated from each other by cracks of a 10–100-nm width.

Au-NPs were synthesized using the well-known citrate method,[24] when a 1% trisodium citrate solution was added to boiling 0.01% chloroauric acid at magnetic stirring, and the mixture was boiled during 20 min. The average diameter of Au-NPs present in the suspension was measured to be 56 ± 1 nm by employing the nanoparticle tracking analysis technique.

To modify Au-NPs with TNB molecules, the Au-NPs suspension was mixed with a 10 mM solution of 5-thio(2-nitrobenzoic acid) in 50 mM HEPES (pH 8) in proportion 2:1 and kept at ambient temperature during the incubation period of 12 hr. Further on, a polyethylene glycole water solution (10 mg/mL) was added to the obtained TNB/Au-NPs suspension in proportion 50:1, the mixture was kept for 1 hr and then centrifugated. After this, the residue was resuspended in a polyethylene glycole water solution (0.5 mg/mL).

To obtain Au-NPs modified by MPBA molecules, the Au-NPs suspension was mixed with a 4-mercaptophenylboronic acid solution in water in proportion 1:1, the mixture was kept at ambient temperature during the incubation period of 1 hr and then centrifugated. The residue was resuspended in water.

Both TNB and MPBA molecules contain a thiol group enabling covalent Au–S bonding of a molecule at the Au-NP surface. The bonds are formed during the incubation period.

To produce SERS-active junctions, the CeO_2 film surface was first covered with a 1% poly(diallyldimethylammonium chloride) water solution to form a polycation monolayer. Then, the surface was rinsed with water and dried out at open air conditions. After that, the substrate with the positively charged CeO_2 film was immersed for 60 min into the suspension of freshly obtained TNB/Au-NP or MPBA/Au-NP conjugates, rinsed with water, and dried out.

During the experiments, all the samples were kept and investigated in open air at ambient temperature.

3 | RESULTS AND DISCUSSION

Examples of scanning electron microscope (SEM) images of a surface of a $CeO_2/Al/Al_2O_3$ sample, having a 1,900 nm-thick CeO_2 film with TNB/Au-NPs deposition, are presented in Figure 2. The dimensions of the surface areas are ~7.5 μm × 4.5 μm (Figure 2a) and ~0.6 μm × 0.4 μm (Figure 2b). Numerous details of the sample surface, such as facets, cracks, and various Au-NP structures, can be clearly distinguished. The TNB-modified Au-NPs are inhomogeneously spread over the film surface in the form of islands, with characteristic transversal dimensions of 500–2,000 nm, as well as of small clusters, dumbbells, or single nanospheres (see Figure 2b). In previous studies,[1,2] the fraction of the CeO_2 film surface occupied by the groups of the TNB-modified Au-NPs at the 2,000-nm thick CeO_2 film was evaluated to be ~5–6%. In the case of the investigated sample with the MPBA-modified Au-NPs, SEM images show that the "filling factor" of Au-NPs is significantly smaller, so the Au-NPs structures, mainly small NP clusters and single NPs, are located much sparsely.

It should be noted that the optical microscope imaging camera, with a 100× 0.6 NA objective, allows the surface faceted structure of the samples under investigation to

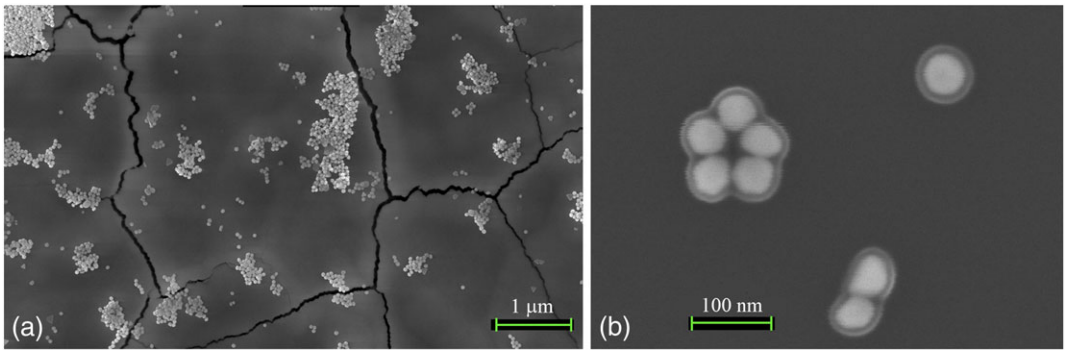

FIGURE 2 Scanning electron microscope images of a $CeO_2/Al/Al_2O_3$ sample surface with the TNB-modified Au-NPs: (a) ~7.5 μm × 4.5 μm and (b) ~0.6 μm × 0.4 μm surface areas [Colour figure can be viewed at wileyonlinelibrary.com]

be distinguished, with the islands of Au-NPs represented as darker spots. Despite the much lower quality of the optical camera images, as compared to the SEM ones, it is sufficient for targeting of the laser beam to a sample area of interest.

The sensitivity of the micro-CARS spectrometer was estimated in the course of recording the epi-signals of CARS (in fact, of two-color four-wave mixing [TCFWM]) in a 2,400-nm CeO_2 film of a $CeO_2/Al/Al_2O_3$ sample without any NPs and reporter molecules at the surface. At average laser powers as small as $P_p \approx 15$ mW (pump power) and $P_S \approx 5$ mW (Stokes power), and exposure of 1 s, the nonresonant anti-Stokes signal obtained at different pump wavelengths $\lambda_p = 910$ nm, 895 nm, and 880 nm that correspond to different Raman frequency shifts ≈1,590 cm^{-1}, 1,780 cm^{-1} and 1,970 cm^{-1}, respectively, and the corresponding anti-Stokes wavelengths $\lambda_{aS} = 795$ nm 772 nm and 750 nm was well above the noise level. The CARS signal amplitudes, recorded by the CCD and normalized by the product ${P^2}_p \times P_S$, were of the order of ~$5{\cdot}10^{-8}$ counts/μW^3. Slight signal variations with λ_p can be attributed to the wavelength dependence of rather the dichroic mirror and the detection path transmittance than that of the CeO_2 film nonlinear susceptibility.

Before detecting Raman-resonant SECARS signals from the samples with deposited reporter molecule/Au-NP conjugates, a threshold of a sample damage by a laser beam was evaluated. The optical damage threshold level was found to be about 200 kW/cm^2 or 2 mW/μm^2 (~$6{\cdot}10^{15}$ photons/μm^2/s) for cw radiation at 633 nm and ≈0.5 mW/μm^2 (~$2{\cdot}10^{15}$ photons/μm^2/s)—for the average intensity of a 85 MHz repetition rate 6 ps pulse sequence at 785 nm. These values were obtained by measuring the 1,338 cm^{-1} TNB line intensity variation in SERS spectra of TNB/Au-NP/$CeO_2/Al/Al_2O_3$ samples under study while gradually increasing pump laser intensity. When the latter exceeds a certain value, the TNB line intensity starts to decrease, and the changes become irreversible. Physical damage of a sample surface that can be observed through the optical microscope occurs at higher power densities.

When discussing the values of sample optical damage threshold, it should be clear that for the particular type of samples, which contain on the surface of the CeO_2 film all the possible types of Au-NPs structures, starting from a single nanosphere and ending by a conglomerate of several hundreds of aggregated NPs (see Figure 2), a single exact value of the optical damage threshold cannot be established experimentally. The reason for this are significant variations that this value experiences from sample to sample, as well as from one point to another within a single sample. In this regard, the term "damage threshold" refers to an estimate of the laser power density value, below which there appears a chance to obtain reproducible SECARS images in a number of consecutive scans.

When performing SECARS measurements, comparable values of sample damage threshold average intensities of the pump laser beams employed (P_p, $P_S \approx 0.2$ mW/μm^2, or ~10^{15} photons/μm^2/s) were obtained. This was done by observing the deviation from a linear dependence of the SECARS signal intensity on the product ${P_p}^2 \times P_S$. It should also be mentioned that for the samples under investigation SECARS mapping of the same sample surface area with gradually (from scan to scan) growing laser power reveals significantly different radiation endurance of the observed spots of strong anti-Stokes signals. For a number of these spots, SECARS signal intensity nicely follows the ${P_p}^2 \times P_S$ dependence up to relatively high power levels, whereas for the other spots, the signal vanishes already at quite low pump intensities. Recently, a special attention was paid to this subject by Pozzi et al.[25]

Additional test measurements, aimed to evaluate SECARS signal intensity, were performed using a $CeO_2/Al/Al_2O_3$ 2,400-nm CeO_2 film sample with unmodified Au-NPs immobilized on its surface. The spatial distribution of epi-CARS (or more precisely, of epi-TCFWM) signals from an area of the sample surface was registered at two pump wavelengths $\lambda_p = 932$ nm and $\lambda_p = 900$ nm.

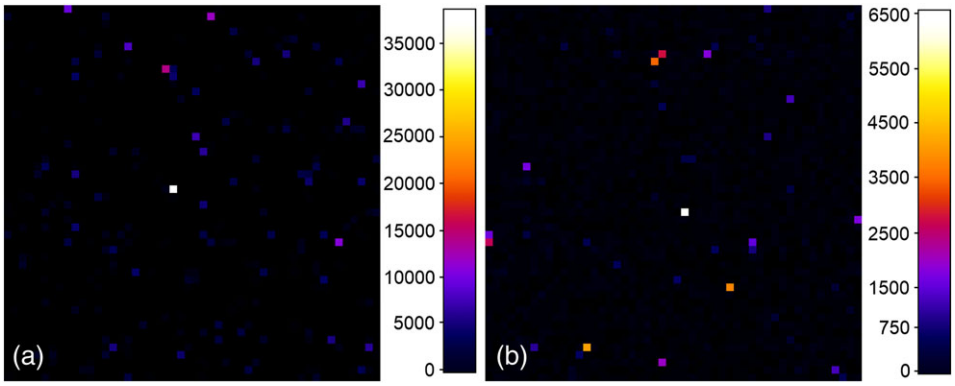

FIGURE 3 Examples of surface-enhanced coherent anti-Stokes Raman scattering signal spatial distributions for unmodified Au-NPs on CeO_2 film surface (40 μm × 40 μm, slow-mapping, step 0.8 μm): (a) λ_p = 932 nm; (b) λ_p = 900 nm. Here and in the following figures, the numbers in the look-up tables correspond to ADC counts [Colour figure can be viewed at wileyonlinelibrary.com]

Selected values of λ_p correspond to the Raman shifts of 1,333 cm^{-1} (resonant with one of the TNB molecule Raman-active transitions) and 1,714 cm^{-1} (nonresonant). In this case, the levels of laser power were reduced down to $P_p \approx 30$ μW and $P_S \approx 52$ μW (i.e., the product $P^2{}_p \times P_S$ became about seven orders of magnitude smaller than that at irradiation of the CeO_2 surface without Au-NPs). During scanning the focused laser spot across the surface areas using the slow-mapping mode with the step of the order of the spot diameter (0.8 μm) very narrow single peaks of strong anti-Stokes signals ("bright spots") were observed. Comparing this to the signals obtained previously without Au-NPs at the film surface, one can assume that the detected signals result from surface-enhanced radiation-metal NP interaction processes.[9,23,26] The examples of spatial distributions of SECARS signals obtained from the same 40 μm × 40 μm (51 × 51 pixels) sample surface area at different λ_p are presented in Figure 3. The rare bright spots of various intensities, with transversal dimensions of one step of the scan and spaced by 10–20 μm, correspond, presumably, to various Au-NP-structures (see Figure 2).[27–29] The signal amplitudes in the bright spots achieve, at 932 nm (λ_{aS} = 828 nm), ~38,800 ADC counts (Figure 3a), whereas at 900 nm (λ_{aS} = 780 nm) they appear to be about six times smaller (Figure 3b), which, among other reasons, can be related to the wavelength dependence of the signal optical path transmittance. The average background signal between the bright spots is ≈55 counts at 932 nm (Figure 3a) and ≈26 counts at 900 nm (Figure 3b). Hence, the SECARS imaging contrast of signal-generating Au-NP structures lies, in this case, in the range of 250–700. At the same time, the obtained values of the SECARS signal amplitudes, normalized by the product $P^2{}_p \times P_S$, are ~0.15–0.87 counts/μW^3. Significant enhancement of Raman nonresonant signal intensity may be provided by TCFWM processes near one- or two-photon absorption resonances within various Au-nanostructures at the CeO_2 film surface.[26] Attention is drawn to the fact that practically no spatial correlation is observed between the microimages obtained with different λ_p (at the respective λ_{aS}). This may be due to the wavelength dependence of the efficiency of a few different elementary processes of four-wave mixing at Au-NP structures of different size and shape, because each of them can contribute to the signal intensity at the same anti-Stokes wavelength.

An example of a SECARS microimage of a 24 μm × 24 μm (251 × 251 pixels) surface area of a $CeO_2/Al/Al_2O_3$ 1,900-nm CeO_2 film sample with a deposition of TNB/Au-NP conjugates is presented in Figure 4. The pump and Stokes radiations at λ_p = 931.5 nm (≈300 μW) and λ_S = 1,064 nm (≈1,000 μW), respectively, corresponding to the Raman shift of 1,338 cm^{-1} of the NO_2 group in TNB molecules, were employed for this record, resulting in the anti-Stokes wavelength λ_{aS} = 828 nm. Because the width of the Raman line in

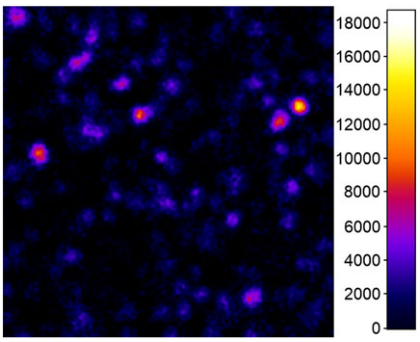

FIGURE 4 Surface-enhanced coherent anti-Stokes Raman scattering Raman resonant microimage of a sample surface area with a deposition of TNB/Au-NP conjugates (24 μm × 24 μm, fast-mapping, step 0.1 μm). The Raman line at 1,338 cm^{-1} of TNB molecules is used [Colour figure can be viewed at wileyonlinelibrary.com]

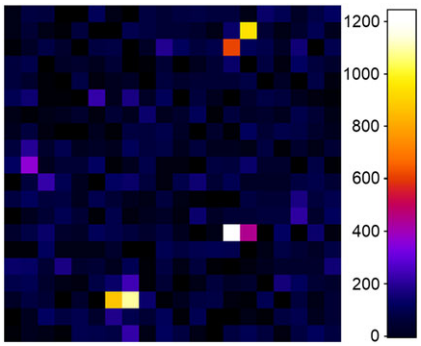

FIGURE 5 Surface-enhanced coherent anti-Stokes Raman scattering Raman resonant microimage of a sample surface area with a deposition of MPBA/Au-NP conjugates (19.3 μm × 19.3 μm, slow-mapping, step 1.0 μm). The Raman line at 1,571 cm^{-1} of MPBA molecules is used [Colour figure can be viewed at wileyonlinelibrary.com]

SERS spectra of TNB/Au-NP conjugates exceeds 20 cm^{-1}, the resonant conditions are not very critical to adjust. The image was accumulated over 30 fast-mapping scans (step 0.1 μm, 1 s/image), and the physical spatial resolution was estimated to be 0.6 μm. The highest Raman-resonant signal amplitude in the bright spots of the image is ~18,800 counts of the 16-bit ADC after the PMT module, whereas the average background signal in between these spots is ≈45 counts for the 30 s accumulation time. This characterizes the high contrast (~400) of the imaging of these conjugates.

An example of a SECARS microimage of a 19.3 μm × 19.3 μm (20 × 20 pixels) 2,400-nm CeO_2 film sample surface area with a deposition of MPBA/Au-NP conjugates is shown in Figure 5. The pump and Stokes radiations at $\lambda_p \approx 913$ nm (≈900 μW) and $\lambda_S = 1064$ nm (≈1,200 μW), corresponding to the Raman line at 1,571 cm^{-1} of MPBA molecules, were employed for the record, providing $\lambda_{aS} \approx 798$ nm. The width of the Raman feature in SERS spectra of MPBA/Au-NP conjugates is ~30 cm^{-1}, and the Raman-resonant conditions are easily achieved as well. The image was recorded using the slow-mapping mode (step 1 μm, 1 s/pixel). The highest Raman-resonant signal amplitude in the bright spots reaches ~1,250 counts of the 16-bit CCD ADC, whereas the average background signal appears to be about 25 counts. Hence, the imaging contrast in this case is ~50. The value of the SECARS signal amplitude, normalized by the product $P^2_p \times P_S$, is ~$1.3 \cdot 10^{-6}$ counts/μW^3.

It is worth mentioning that the characteristic transversal dimensions of the bright spots (width of the intensity profile of its horizontal or vertical cross section) are ≈0.6–0.8 μm—a bit less than the pump and Stokes beam spot diameters. This can be explained by the small dimensions of the scattering sites at the surface and the nonlinear character of the four-wave mixing (CARS) process involved. It should be noted that in both presented microimages, the bright spots are found quite rarely, similar to the case of NPs without reporter molecules (see Figure 3).

SECARS microimages of the same 40 μm × 40 μm (51 × 51 pixels) surface area of a $CeO_2/Al/Al_2O_3$ 1,900-nm CeO_2 film sample with a deposition of TNB-modified Au-NPs, recorded at TNB Raman-resonant and nonresonant pump wavelengths, $\lambda_p = 932$ and $\lambda_p = 900$ nm, are presented in Figure 6. Laser powers $P_p \approx 30$ μW and $P_S \approx 52$ μW and the slow-mapping mode (step 0.8 μm, 1 s/pixel) were used for the recording. The images can be qualitatively and quantitatively compared with those recorded at the same wavelengths for unmodified Au-NPs on CeO_2 film surface (see Figure 3). The slow-mapping mode was used to obtain these images because, for the sake of reproducibility, the mapping was performed at the lowest possible pump laser powers, whereas, as it was mentioned above, the sensitivity of the detection

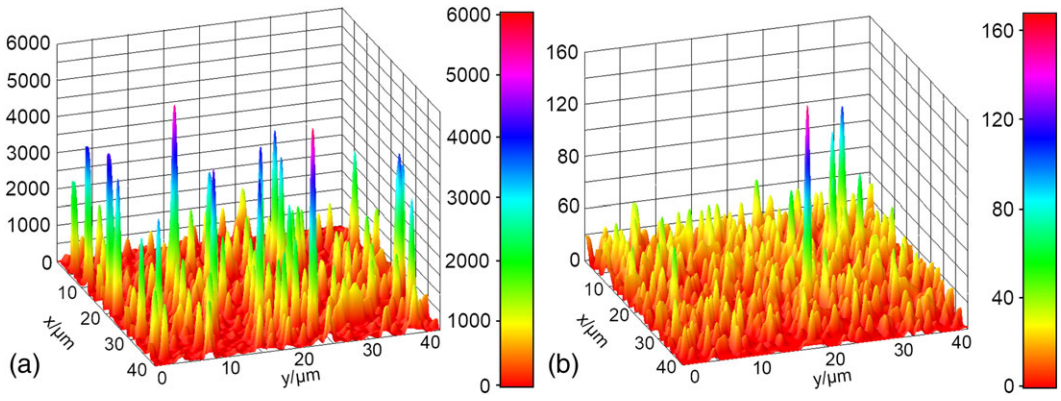

FIGURE 6 Surface-enhanced coherent anti-Stokes Raman scattering microimages of TNB/Au-NPs on CeO_2 film surface (40 μm × 40 μm, slow-mapping, step 0.8 μm): (a) $\lambda_p = 932$ nm (the Raman line at 1,333 cm^{-1}); (b) $\lambda_p = 900$ nm [Colour figure can be viewed at wileyonlinelibrary.com]

channel with the CCD is about 100 times higher than that with the PMT.

In the nonresonant excitation case (Figure 6b), a few small transversal dimension (one step) bright spots were observed—similar to the case of the unmodified Au-NPs (Figure 3b). The highest signal amplitude in the bright spots reached only ~170 ADC counts, and the average background signal was ~6 counts, resulting in the imaging contrast ~30. The value of this SECARS signal amplitude, normalized by the product $P^2_p \times P_S$, is ~$3.6{\cdot}10^{-3}$ counts/μW^3. As in the case of the unmodified Au-NPs, the rare bright spots may be provided by TCFWM processes enhanced by one- or two-photon resonances within various TNB-modified Au-nanostructures at the CeO_2 film surface.

In the Raman resonant excitation case (Figure 6a), significantly larger number of bright spots, with a broader range of amplitudes, was recorded that is quite opposite to the case of the unmodified Au-NPs (Figure 3a). As in Figure 3, there is no spatial correlation between the two images. The highest signal amplitude in the bright spots reached ~6,000 ADC counts (the average background signal was ~25 counts), and the imaging contrast was ~240. The value of the peak SECARS signal amplitude, normalized by the product $P^2_p \times P_S$, is ~0.13 counts/μW^3. Hence, the ratio of maximal amplitudes in Figure 6a,b is ~35, compared to ~6 in the case of the unmodified Au-NPs (Figure 3). As a result, one can assume that, contrary to the case represented in Figure 3a, where rare Raman-nonresonant anti-Stokes signals can be generated only by the Au-NP structures, very large density of bright spots and their relatively high intensity are most likely due to Raman-resonant SECARS by TNB molecules.

As it was mentioned above, in the particular setup employed the geometrical beam paths are exactly the same for the detected anti-Stokes CARS and Stokes Raman radiation, the only difference in the detection efficiency coming from the dispersion of optical properties of the involved optics and the detector. Hence, it is of interest to record SECARS and SERS microimages of the same surface area of a $CeO_2/Al/Al_2O_3$ sample with the modified Au-NPs in order to observe the spatial correlation (if any) of their signal intensity and to compare the imaging contrast.

Figure 7 shows examples of 29 μm × 29 μm (30 × 30 pixels) microimages of the same area of a sample surface for MPBA-modified Au-NPs. A slow-mapping mode (step 1 μm, 1 s/pixel) SECARS image at λ_p = 912 nm (1,571 cm^{-1}), recorded at ≈0.3 mW (λ_p) and ≈1.2 mW (λ_S) (or totally about $8{\cdot}10^{15}$ photons/μm^2/s), and a SERS image at λ_p = 785 nm (≈1.0 mW, or $4{\cdot}10^{15}$ photons/μm^2/s), with the signal integration near λ_S = 895 nm, are presented. SECARS signal amplitudes, normalized by the product $P^2_p \times P_S$, amount in this case only ~$2.9{\cdot}10^{-5}$ counts/μW^3. The images show good correlation of the signal spatial distributions. As far as the imaging contrast is concerned, in SECARS, it is ~50, whereas in SERS, it is only ~7, the average backgrounds being at the similar level: ~60 and ~40 counts, respectively. The origin of the higher background-to-signal ratio in SERS is unclear and is an interesting point for further investigations, because between the bright spots, there should be practically no Au-NPs which could potentially deliver nonresonant electronic Raman scattering.[23]

On the other hand, similar slow-mapping mode SECARS and SERS microimages for TNB-modified Au-NPs recorded, using the Raman line at 1,338 cm^{-1}, with ≈0.3 mW (λ_p), ≈1.0 mW (λ_S) and with ≈1.0 mW (λ_p = 785 nm), demonstrate that there is practically no spatial correlation between the images. The normalized SECARS signal amplitudes are larger in this case and amount ~$7.0{\cdot}10^{-4}$ counts/μW^3. The imaging contrasts in SECARS and SERS are comparable to those obtained with MPBA/Au-NP conjugates: ~50 and ~9, whereas the

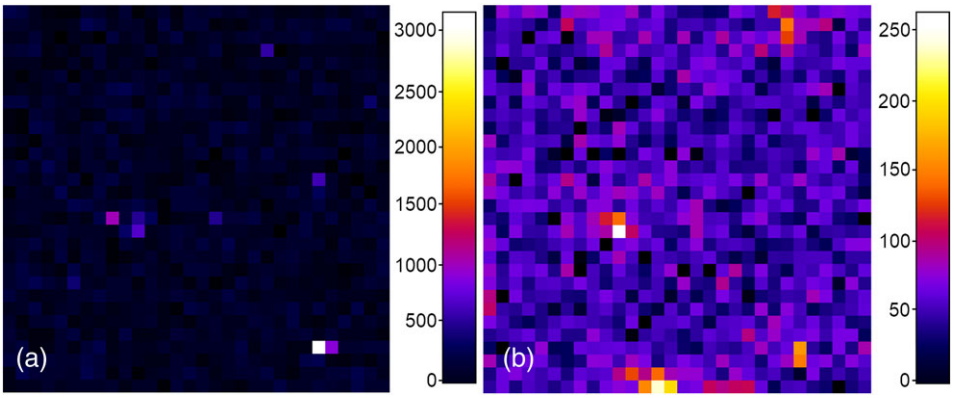

FIGURE 7 Microimages of the same spatial area (29 μm × 29 μm, slow-mapping mode, step 1 μm) of an MPBA/Au-NP/$CeO_2/Al/Al_2O_3$ sample using the Raman line at 1,571 cm^{-1}: (a) coherent anti-Stokes Raman scattering, λ_p = 912 nm; (b) surface-enhanced Raman scattering , λ_p = 785 nm, λ_S = 895 nm [Colour figure can be viewed at wileyonlinelibrary.com]

average backgrounds are quite different: ~1,200 and ~250 counts, respectively. The reason for the absence of the correlation might be, for example, that, as it was discussed above, the SECARS signals are generated not only by Au-NP-bound TNB molecules, such as in SERS, but also by the Au-NP-structures themselves. For the investigated sample with Au-NPs modified by TNB molecules, these structures have a significantly higher surface density at the CeO_2 film and a larger variety of dimensions and shapes. Another reason might be related to the fact that SECARS and SERS signals are generated by local fields at different wavelengths. Hence, these fields may be enhanced by the Au-NPs with different efficiency because of distinctive wavelength dependence of the gain provided by Au-NP structures of diverse size. In any case, the weak correlation of SECARS and SERS signals is an object of further investigations.

4 | CONCLUSION

The experimental results reported in this work demonstrate for the first time the feasibilities to detect epi-SECARS signals from thionitrobenzoic acid, TNB, and mercaptophenylboronic acid, MPBA, reporter molecules bound to Au-NPs, which are immobilized on the surface of a faceted dielectric CeO_2 film/Al structure, by employing a newly built scanning confocal picosecond near-infrared laser-based micro-CARS spectrometer.

The sensitivity of the spectrometer in relation to the novel metamaterial samples under study was investigated, and a level of signal detection was estimated. The range of TNB(MPBA)/Au-NP/CeO_2/Al/Al_2O_3 samples nondestructive excitation laser powers was evaluated.

SECARS signal mapping of a CeO_2 film surface with immobilized Au-NP structures, unmodified by reporter molecules, was performed at different wavelengths for the same sample surface area, and signal spatial distributions were examined. Further on, Raman resonant and nonresonant SECARS microimages of TNB- and MPBA-modified Au-NP structures on a CeO_2 film surface were obtained and compared, and the imaging contrasts were estimated. Finally, Raman resonant SECARS and SERS microimages of the same surface area of the metamaterial samples with TNB- and MPBA-modified Au-NP structures were recorded and considered in terms of image spatial correlation and imaging contrast.

The investigations showed that at Raman resonant two-color laser excitation of organic reporter molecules bound to Au-NPs on the CeO_2 film surface strong SECARS signals can be generated with laser powers not destroying the organic-metal conjugates. SECARS microimages of sample surfaces demonstrated a large chemical imaging contrast up to 400. The excellent imaging contrast obtained promises a high SECARS detectability of the reporter molecules at the surface of the novel Au-NP/CeO_2/Al metamaterial. In addition, the study demonstrated that CARS signals from the CeO_2 film surface with unmodified Au-NP structures result mainly from surface-enhanced four-wave mixing processes assisted by Au-nanostructures. These signals have a high-contrast spatial distribution depending on the excitation wavelengths.

Further research will be directed towards a study of the limits of SECARS signal sensitivity to the probed reporter molecules and a comparison of their detectability by using SECARS and SERS at the surface of the metamaterial under investigation. The origin of Raman nonresonant SECARS signals and spatial correlation of SECARS and SERS from the same sample surface area will be an object of investigations as well.

ACKNOWLEDGEMENTS

The work was financially supported by the Basic Research Program of the Presidium of Russian Academy of Sciences "Supersensitive sensors and field hyper-amplification by optical metamaterials" № I.16 and by the Thematic Project "Multimodal optical platform for condensed matter studies" of the Joint Institute for Nuclear Research. The authors are grateful to E. D. Obraztsova and S. N. Bokova-Sirosh for the support in recording sample Raman and SERS spectra at the Natural Sciences Center of A.M. Prokhorov General Physics Institute, Russian Academy of Sciences. Providing the opportunity to record sample SEM images at the Research & Education Centre "Functional Micro/Nanosystems" (FMNS REC. ID 74300) of Bauman Moscow State Technical University is gratefully acknowledged.

ORCID

Dimitrii N. Kozlov http://orcid.org/0000-0002-2868-9554
Konstantin A. Vereschagin http://orcid.org/0000-0002-1561-0341

REFERENCES

[1] I. Kurochkin, I. Ryzhikov, A. Sarychev, K. Afanasiev, I. Budashov, M. Sedova, I. Boginskaya, S. Amitonov, A. Lagarkov, *Advanced Electromagnetics* **2014**, *3*, 57.

[2] I. N. Kurochkin, I. A. Ryzhikov, A. K. Sarychev, K. N. Afanasiev, I. A. Budashov, M. V. Sedova, I. A. Boginskaya, S. V. Amitonov, E. V. Korostilev, A. N. Lagarkov, *Moscow Univ. Chem. Bull. (Engl. Transl.)* **2015**, *70*, 102.

[3] C. K. Chen, A. H. B. de Castro, Y. R. Shen, F. DeMartini, *Phys. Rev. Lett.* **1979**, *4*, 946.

[4] D. S. Chemla, J. P. Heritage, P. F. Liao, E. D. Isaacs, *Phys. Rev. B* **1983**, *27*, 4553.

[5] E. J. Liang, A. Weippert, J.-M. Funk, A. Materny, W. Kiefer, *Chem. Phys. Lett.* **1994**, *227*, 115.

[6] H. Chew, D.-S. Wang, M. Kerker, *J. Opt. Soc. Am. B* **1984**, *1*, 56.

[7] J. Brocious, E. O. Potma, *Mater. Today* **2013**, *16*, No 9, 344.

[8] D. Lis, F. Cecchet, *Beilstein J. Nanotechnol.* **2014**, *5*, 2275.

[9] N. L. Gruenke, M. F. Cardinal, M. O. McAnally, R. R. Frontiera, G. C. Schatza, R. P. Van Duyne, *Chem. Soc. Rev.* **2016**, *45*, 2263.

[10] T. Ichimura, N. Hayazawa, M. Hashimoto, Y. Inouye, S. Kawata, *J. Raman Spectrosc.* **2003**, *34*, 651.

[11] C. Steuwe, C. F. Kaminski, J. J. Baumberg, S. Mahajan, *Nano Lett.* **2011**, *11*, 5339.

[12] D. V. Voronine, A. M. Sinyukov, X. Hua, E. Munusamy, G. Ariunbold, A. V. Sokolov, M. O. Scully, *J. Modern Optics* **2015**, *62*, No. 2, 90.

[13] X. Hua, D. V. Voronine, C. W. Ballmann, A. M. Sinyukov, A. V. Sokolov, M. O. Scully, *Phys. Rev. A* **2014**, *89*, 043841.

[14] S. Schlücker, M. Salehi, G. Bergner, M. Schütz, P. Ströbel, A. Marx, I. Petersen, B. Dietzek, J. Popp, *Anal. Chem.* **2011**, *83*, 7081.

[15] T.-W. Koo, S. Chan, A. A. Berlin, *Opt. Lett.* **2005**, *30*, No. 9, 1024.

[16] A. Fast, J. P. Kenison, C. D. Syme, E. O. Potma, *Appl. Optics* **2016**, *55*, No. 22, 5994.

[17] H. Kim, D.-Y. Kim, K.-I. Joo, J.-H. Kim, S. M. Jeong, E. S. Lee, J.-H. Hahm, K. Kim, D. W. Moon, *Sci. Rep.* **2017**, *7*, https://doi.org/10.1038/s41598-017-09571-w.

[18] Z. Yu, Y.-R. Zhen, O. Neumann, J., K. Day, P. Nordlander, N. J. Halas, *Nature Communications* **2014**, *5*, 4424.

[19] S. Yampolsky, D. A. Fishman, S. Dey, E. Hulkko, M. Banik, E. O. Potma, V. A. Apkarian, *Nature Photonics* **2014**, *8*, 650.

[20] J. He, C. Fan, P. Ding, S. Zhu, and, E. Liang. *Sci. Rep.* **2016**; *6*, 20777.

[21] J. Wang, J. Zhang, Y. Tian, C. Fan, K. Mu, S. Chen, P. Ding, E. Liang, *Opt. Express* **2017**, *25*, No. 1, 497.

[22] Z. Zhang, G. Song, *J. Semiconductors* **2017**, *38*, No. 2, 022001.

[23] K. T. Crampton, A. Zeytunyan, A. S. Fast, F. T. Ladani, A. Alfonso-Garcia, M. Banik, S. Yampolsky, D. A. Fishman, E. O. Potma, V. A. Apkarian, *J. Phys. Chem. C* **2016**, *120*, 20943.

[24] J. Turkevich, P. C. Stevenson, J. Hillier, *Discuss. Faraday Soc.* **1951**, *11*, 55.

[25] E. A. Pozzi, N. L. Gruenke, N. Chiang, D. V. Zhdanov, N. Jiang, T. Seideman, G. C. Schatz, M. C. Hersam, R. P. Van Duyne, *J. Phys. Chem. Lett.* **2016**, *7*, 2971.

[26] Y. Wang, C. –Yu Lin, A. Nikolaenko, V. Raghunathan, E. O. Potma, *Adv. Opt. Photonics* **2011**, *3*, 1.

[27] C. J. Addison, S. O. Konorov, A. G. Brolo, M. W. Blades, R. F. B. Turner, *J. Phys. Chem. C* **2009**, *113*, 3586.

[28] F. Yu Zhanga, Y.-R. Wen, P. N. Zhena, N. J. Halasa, *PNAS.* **2013**, *110*, 9215.

[29] J. Li, I. W. Schie, J. Qian, S. He, T. Huser, *Chemphyschem* **2013**, *14*, 1951.

How to cite this article: Fabelinsky VI, Kozlov DN, Orlov SN, et al. Surface-enhanced micro-CARS mapping of a nanostructured cerium dioxide/aluminum film surface with gold nanoparticle-bound organic molecules. *J Raman Spectrosc*. 2018. https://doi.org/10.1002/jrs.5333